Numerical investigation of lateral jet interaction effects on the hypersonic quasi-waverider vehicle

4 authors, including:

Numerical investigation of lateral jet interaction effects on the hypersonic quasi-waverider vehicle

Dong Chai[1], Yang-Wang Fang[2], Wei-Shi Peng[2] and Peng-Fei Yang[2]

Abstract

Numerical simulations are carried out to investigate lateral jet interaction effects for the hypersonic quasi-waverider vehicle. A reasonable jet nozzles layout is proposed. Based on three-dimensional viscous compressible Reynolds Averaged Navier-Stokes codes, comparisons of the jet interaction flow structures between quasi-waverider vehicle and general axisymmetric vehicle are conducted. Furthermore, the effects of lateral jet control are examined for different angles of attack and free-stream Mach numbers. From detailed flow structure and pressure distribution analysis, the quasi-waverider vehicle gets a better effect of lateral jet without "wrap-around" the body. With the increase in angle of attack or free-stream Mach number, the attitude control moment reduces and the effect of lateral jet decreases.

Introduction

Higher agility and maneuverability would be required in various practical areas for future flight vehicles. Such demands can be effectively realized via the reaction jet control system, which provides a lateral thrust and moment to conduct attitude or orbit control. Compared with conventional aerodynamic controls, reaction jet control systems have the merits of fast response, without aerodynamic heating effect, and of compact design. Thus, it has been widely applied in various vehicles such as spacecraft, missile, satellite, etc.[1–3] However, as the flight vehicle operating in endo-atmospheric space, the lateral jet exhausting into free stream can generate strong interaction resulting in force and moment with complex flow field around the jet. As shown in Figure 1, the lateral jet interaction (JI) can produce complicated flow structure consisting of separation and reattachment on the boundary layer, bow shock, separation shock, barrel shock, and Mach disc.[4] In addition to these features, counter-rotating horseshoe vortices and wake vortices are also shown.

Great efforts have been made on lateral JI effects. For the projectile or missile configurations, Zhang et al.[5] investigated numerically the effects of jet nozzle shapes on the reaction force. The comparison of four kinds of jet nozzle shapes shows that the elliptical one, generating larger separation region ahead of the jet orifice, improves the efficiency of lateral control. Lee et al.[6] developed a three-dimensional (3D) Navier-Stokes code to study the behavior of normal force and pitching moment characteristics for different angles of attack and spouting jet angles. DeSpirito[7,8] simulated computationally the flow interaction effects from the steady jet and transient jet issuing into crossflows for a basic fin-stabilized projectile. Stahl et al.[9,10] conducted pressure measurements on generic missile models with cold and hot side jets. The shock structure was shown with Schlieren images, and the wall streamlines were visualized with oil flow technique.

The studies stated above are focused on general axisymmetric (GA) vehicle configurations. However, as the hypersonic technology matured, the hypersonic vehicle powered by scramjet in waverider

[1]Department of Flight Vehicle and Power Engineering, School of Aeronautics and Astronautics Engineering, Air Force Engineering University, Xi'an, PR China
[2]Department of Aerospace Weapon Engineering, School of Aeronautics and Astronautics Engineering, Air Force Engineering University, Xi'an, PR China
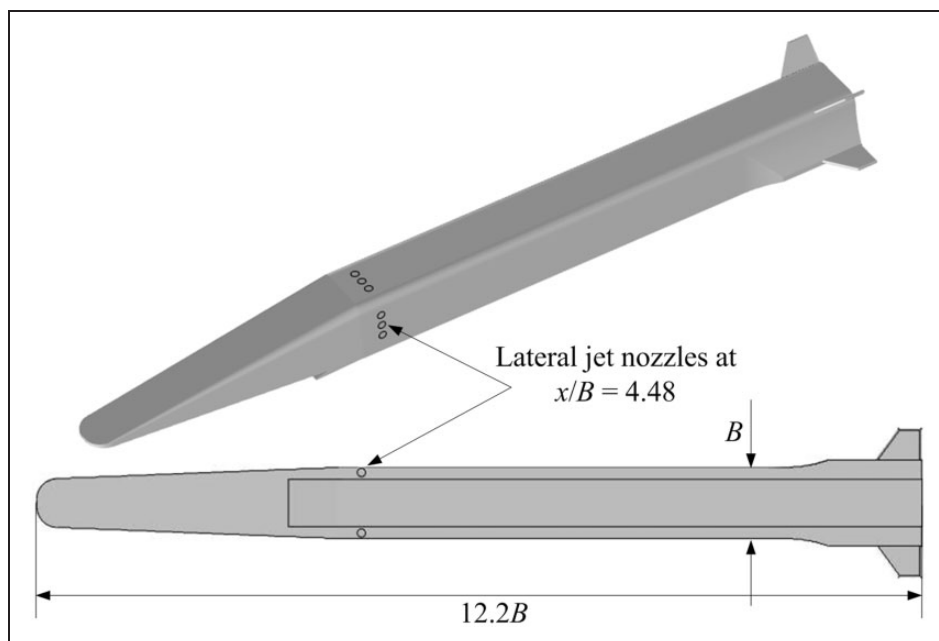
Corresponding author:
Dong Chai, School of Aeronautics and Astronautics Engineering, Air Force Engineering University, Room 405, Department 2, No. 1, Baling Road, Baqiao District, Xi'an 710038, China.
Email: chaidong2012@gmail.com
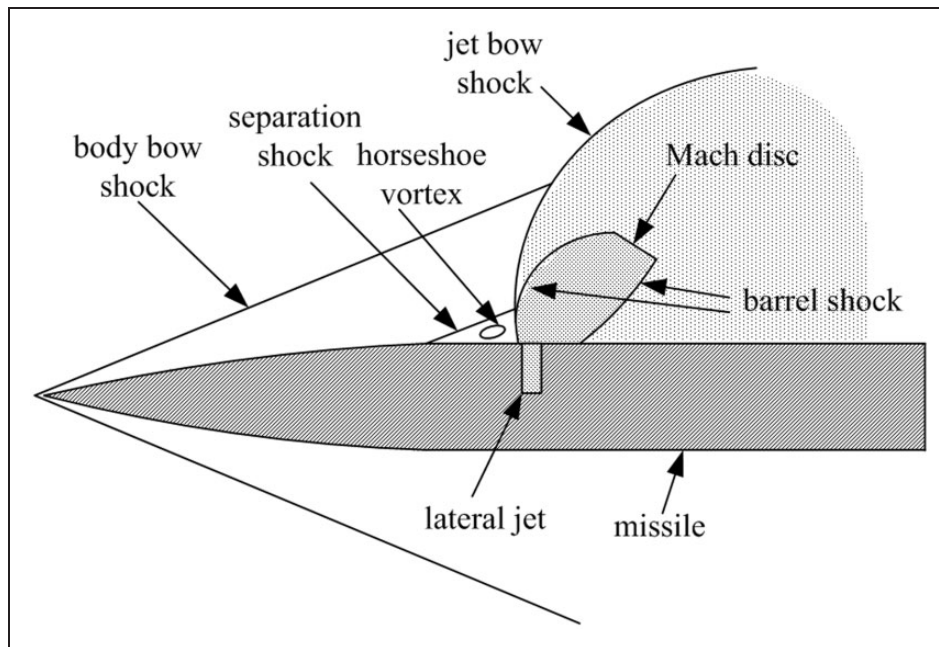
Figure 1. Schematic of lateral jet interaction flow field.

**Figure 2.** Schematic of QW vehicle and jet nozzles layout.

configuration is becoming the focal weapon of various countries. The use of lateral jet control in this type of vehicle similarly entails higher agility and maneuverability. In view of the influence on flow field of scramjet inlet, it is significant to design a proper layout on jet nozzles and investigate the effect to lateral control efficiency of waverider configuration.

This paper focuses on analyzing the lateral JI effects of a hypersonic quasi-waverider (QW) vehicle. Jet nozzles layout is proposed reasonably at first. Then the flow field structure of JI is simulated numerically by 3D viscous compressible Reynolds-Averaged Navier-Stokes (RANS) codes, and comparisons of the

Table 1. Flow conditions of simulation.

Case no.	M_∞	P_{oj}/P_∞	T_t, K	M_J	$\alpha, °$
Case 1	3.0	200	280	1	0
Case 2	3.0	100	295	1.2	0
Case 3	5.0	100	295	1.2	−10, 0, 10
Case 4	6.0	100	295	1.2	0

JI flow between GA and QW are clarified in detail. Finally, the effects of lateral jet control are investigated for different angles of attack and free-stream Mach numbers.
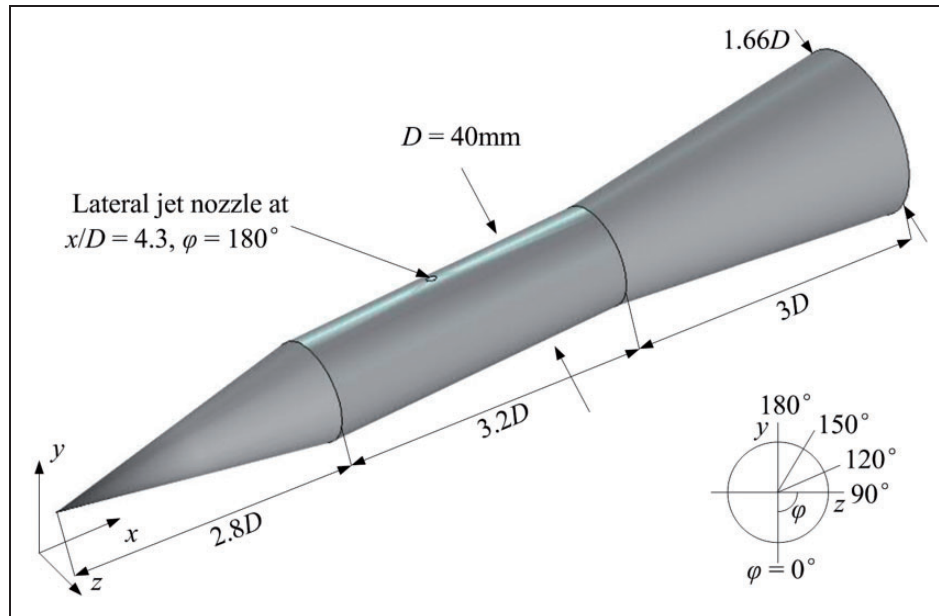
Figure 3. The geometric model and dimensions of GA vehicle.
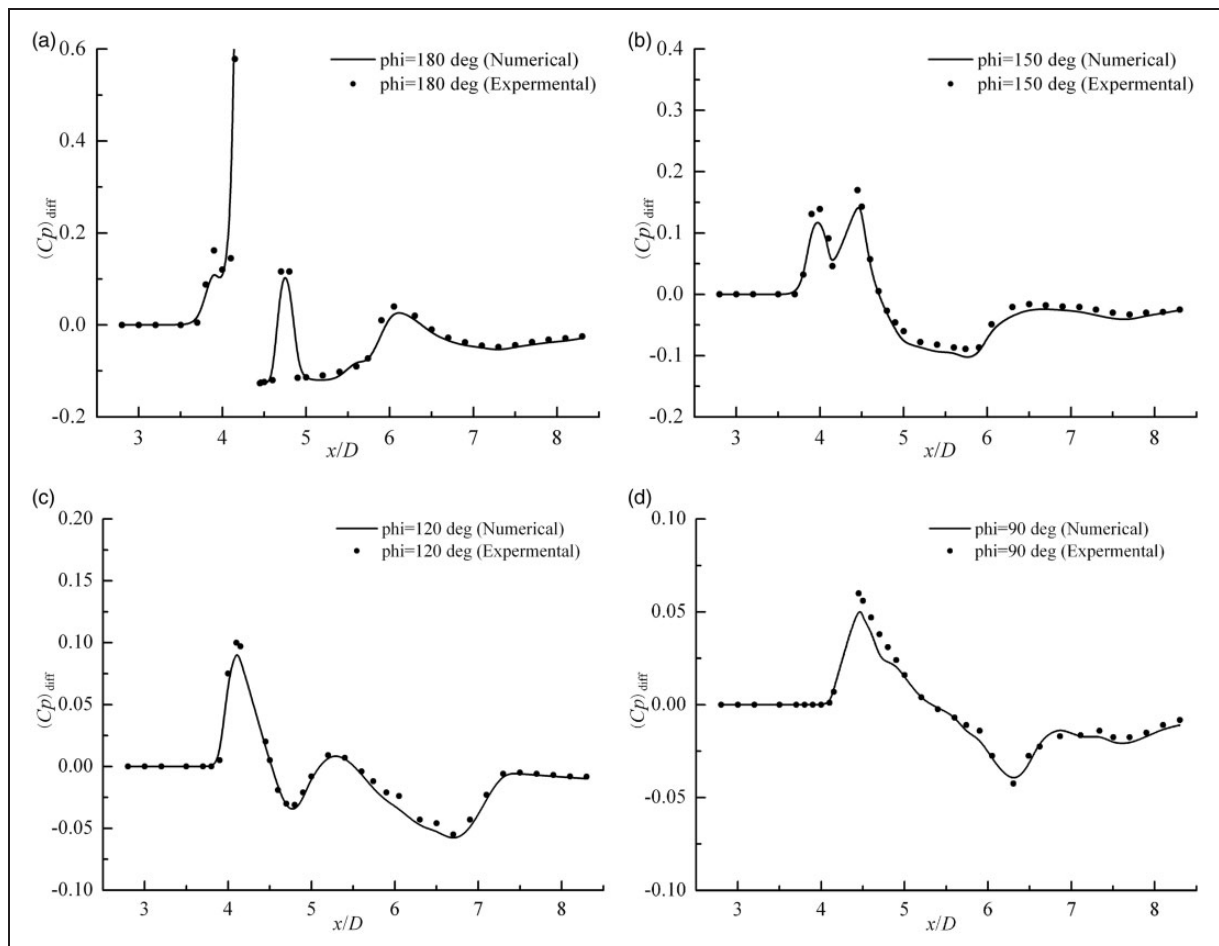
Figure 4. Comparison of pressure distribution along the axial. (a) $\varphi = 180$; (b) $\varphi = 150$; (c) $\varphi = 120$ and (d) $\varphi = 90$.
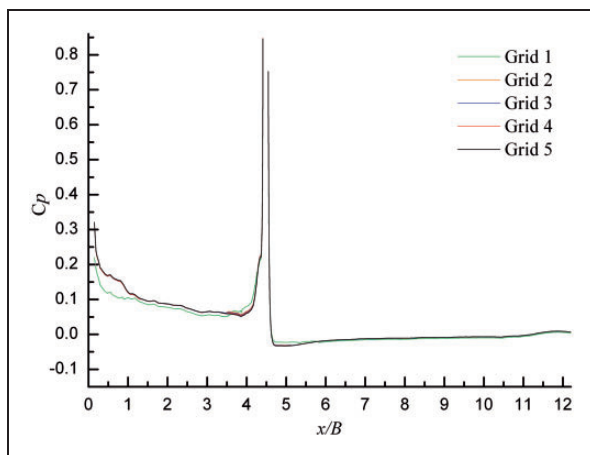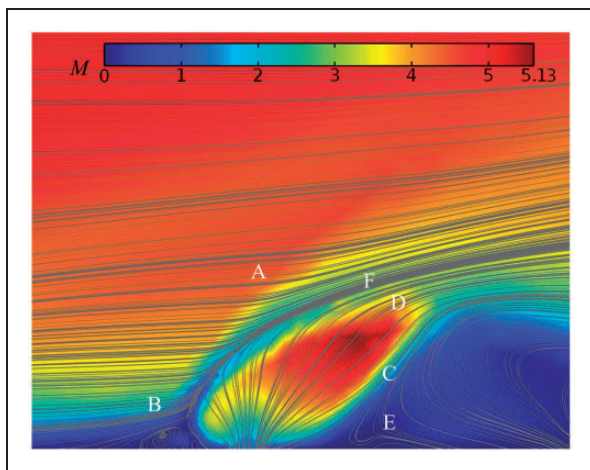
Table 2. Grid sensitivity statistics for GCI study.

Grid number	Cell numbers	CPU time (h)	GCI relative error (%)
1	596,875	4.2	
2	895,312	6.5	5.762
3	1,342,968	11.4	0.976
4	2,014,453	18.8	0.625
5	3,021,680	25.3	0.128

GCI: grid-convergence-index.

Figure 5. Comparison of pressure distribution for different grids.

Figure 6. Jet flow field structure near the orifice.

The jet nozzles layout on QW vehicle

The vehicle configuration we conduct in this paper is based on quasi X-51A waverider vehicle, in which the fuselage has a maximum breadth of $B = 35$ mm. As is presented in Figure 2, three circular lateral jet nozzles, with diameter of $d = 4$ mm, are located on all around the foreside of the fuselage at a position of $x = 4.48B$ downstream from the nose, except the underside. To avoid disturbing the scramjet inlet,
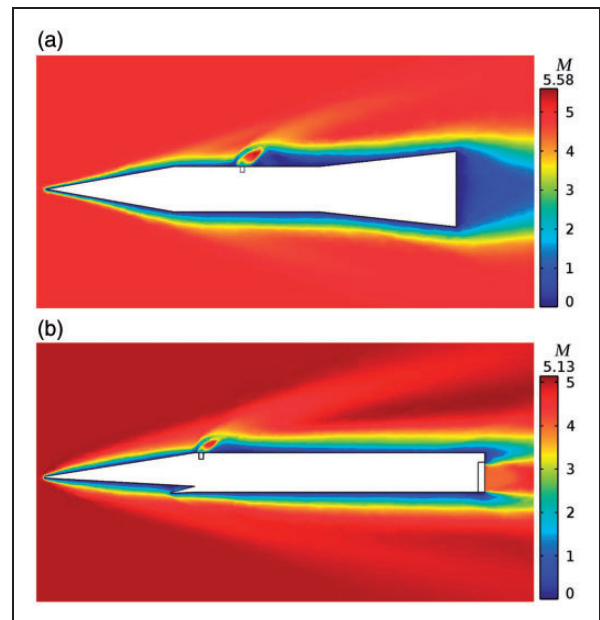
Figure 7. Mach number distribution for different vehicles.

two downward jet nozzles are distributed in both sides of the inlet.

Computational methodology and conditions

The coupled implicit RANS equations and the Spalart-Allmaras one-equation turbulent model are adopted in numerical simulation of the complex flow field with lateral JI phenomena. The second-order upwind difference scheme with the advection upstream spitting method flux vector splitting is utilized to disperse RANS equations. The implicit LU-SGS method is employed for time integration. The Spalart–Allmaras one-equation turbulence model is selected due to its less computational demand. The non-slip and adiabatic wall boundary conditions are adopted for the present calculations. Free-stream Reynolds number is 1.9 million for all cases. The angle of incidence in all cases is 90°, that is, the jet flow of nozzle exit is normal direction. Other boundary conditions and initial field conditions are based on specified parameters, which are listed in Table 1.

The paper is devoted to investigate JI effects, as limited to a single upward jet working. In order to validate the effectiveness and efficiency of the computational fluid dynamics (CFD) model and solving method, the JI flow field of GA vehicle was also simulated and compared with the experimental measurement results of Stahl et al.[9] The geometric model and dimensions are shown in Figure 3, where the diameter of lateral jet nozzle is 0.1 D.

The conditions in Case 1, which can be seen from Table 1, are only set up for GA vehicle to implement the validation. The initial flow parameters correspond with the experiment in Stahl et al.[9] The JI flow
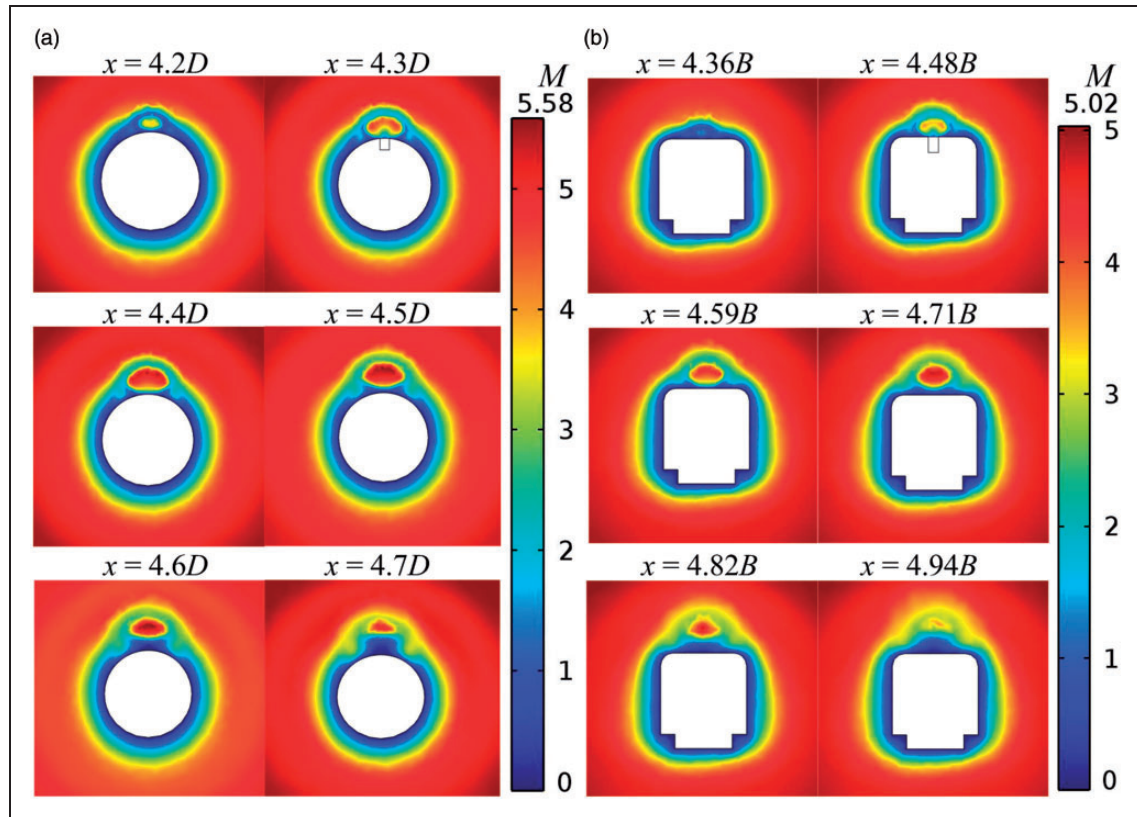
Figure 8. Mach number distribution for different cross sections. (a) axisymmetric and (b) quai-waverider.
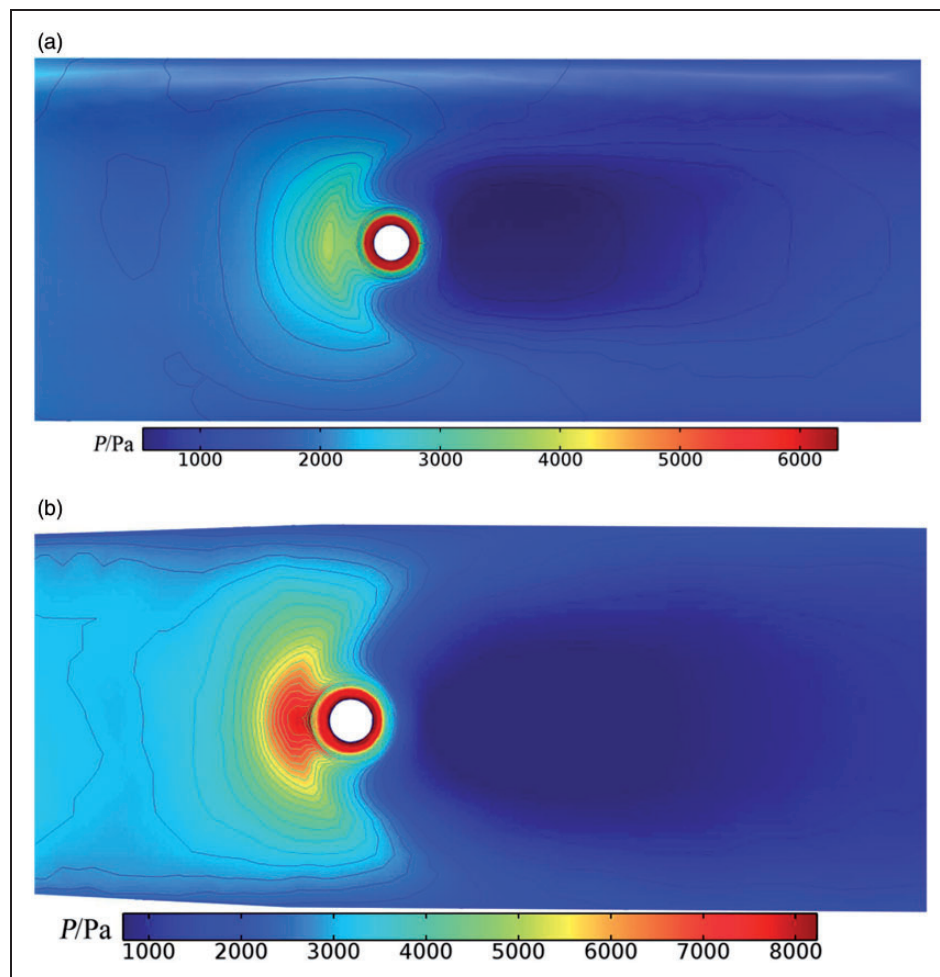
Figure 9. Pressure contours near the orifice for different vehicles. (a) axisymmetric and (b) quai-waverider.

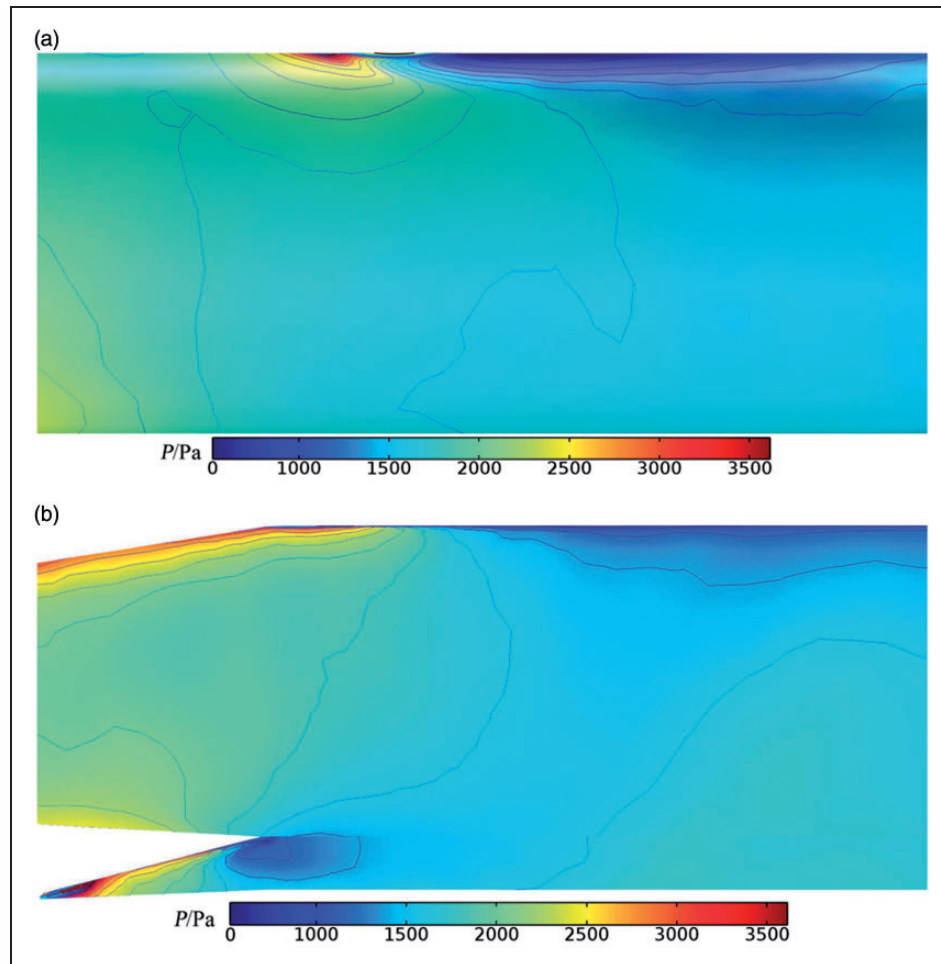**Figure 10.** Side-view wall pressure contours. (a) axisymmetric and (b) quai-waverider.

structures are compared between GA and QW vehicle at the same conditions in Case 3. Simulations were also carried out in this case to investigation JI effects for three different angles of attack, namely, $-10°$, $0°$, and $10°$. To determine the free-stream Mach number effect, Cases 2–4 were performed for three different Mach numbers.

Two 3D structural grid systems with multi-block[11] were generated severally for both types of vehicle, and mesh refinement was conducted at the jet injection region and near the boundary of vehicles, whereas coarser grids were used in the far field region to improve the efficiency of computation. The cell numbers of GA and QW grid systems are 2,763,905 and 3,021,680, respectively.

Results and discussion

Validation example

To verify the CFD procedure, the simulation of JI for GA vehicle was implemented in Case 1. Using the pressure data, the coefficient could be calculated as $C_p = 2(P - P_\infty)/(P_\infty \gamma M_\infty^2)$. In fact, what we focus on is the influence of the lateral jet with the incoming flow. For this purpose, the pressure coefficient

difference between with and without jet was defined, namely, $(C_p)_{\text{diff}} = (C_p)_{\text{with jet}} - (C_p)_{\text{without jet}}$. The axial distributions of calculated pressure coefficient difference at different azimuth angles, which are $180°$, $150°$, $120°$, and $90°$, were compared with experimental values of Stahl et al.[9] in Figure 4. The free steam conditions of this experiment are the same as Case 1.

Plenty of similarity was obtained obviously between computational results and experimental data from Figure 4. The tendency that the high pressure region is in front of the orifice, while the low pressure region behind, was presented for all of the azimuth angles. Furthermore, the peaks of the high and low pressure get lower with the decrease of azimuth angle and the farther from the orifice, namely, the effects of lateral jet get weaker. Meanwhile, the peak points shift backward, as the azimuth angle decreases. This is because the vortices generated by JI wrap around the missile rearward, where the region of vortices is high pressure and the one behind the vortices is low pressure.

The comparison as presented above shows reasonable results from the CFD procedure, that is, the CFD model and solving method are reliable. On the premise that we could not validate all the cases by experiment, the simulated results hereafter are acceptable in
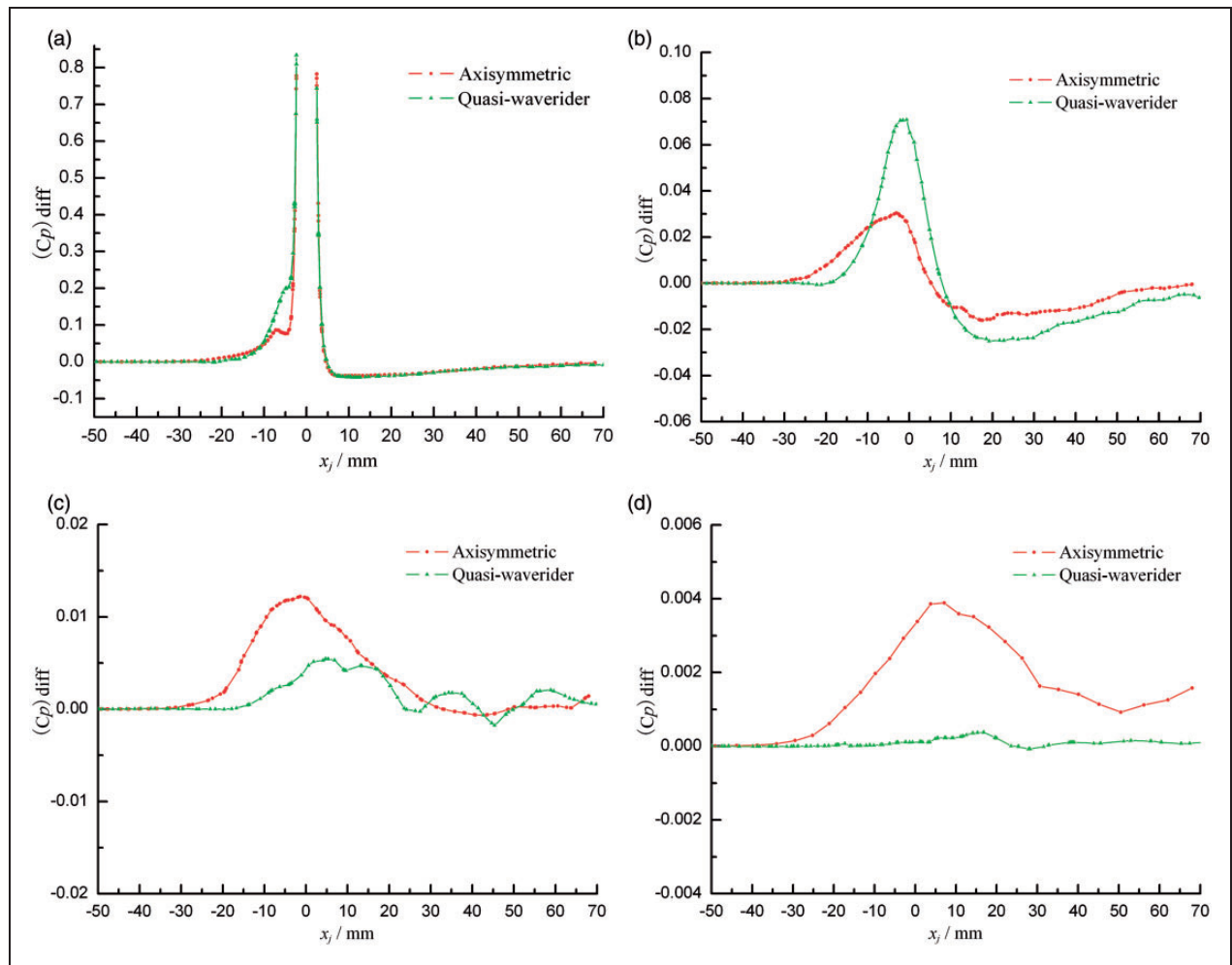
Figure 11. Comparison of pressure distribution for different vehicles. (a) $\varphi = 180$; (b) $\varphi = 150$; (c) $\varphi = 120$ and (d) $\varphi = 90$.

terms of using the same turbulence model and solving method.

The grid convergence study is conducted for JI computational model of QW vehicle in Case 3 via grid-convergence-index (GCI), which is a measure of relative error in the grid. GCI is calculated by generalized Richardson extrapolation[12] and is recognized as the effective way to analyze grid uncertainty. Several grids and there cell numbers are listed in Table 2. Every successive grid is refined with a factor of 1.5.

C_p along the axial direction at 180° azimuth angles by different grids are presented in Figure 5. The values are very close for grid 3-5, and the GCI relative errors are 0.976%, 0.625%, and 0.128%. Finally, the grid 5 is chosen for JI study of QW vehicle.

Flow field structure analysis

The detailed jet flow field structure near the orifice in the injection plane ($\varphi = 180°$) of the QW vehicle, as carried out in Case 3 for 0° angle of attack, is shown in Figure 6. The bow shock (A) is produced upstream of the orifice due to the jet acting as an obstacle to the incoming flow. The flow velocity decreases sharply after passing through the bow shock. On account of the adverse pressure gradient before the jet, the boundary layer is separated to create separation shock in this region. Then the separation shock interacts with the bow shock, leading to a weaker λ-shock structure (B) which produces a vortex structure inside it. The barrel shock (C) encircles the jet plume and is terminated in a Mach disc (D). This strong shock system leads to a flow separation downstream of the orifice and then induces wake vortices (E). A mixing layer (F), as streamlines aggregated distinctly, is established between the lateral jet flow and free stream.

For the comparison of JI effects between GA and QW vehicles, simulations were conducted in Case 3 for 0° angle of attack. The Mach number distributions for $\varphi = 180°$ are shown in Figure 7. The GA vehicle has a larger jet influencing region compared with the QW vehicle. Figure 8 presents the Mach number distributions for different cross sections in front and behind the orifice. The jet influencing region expands with the cross section position moving backwards.
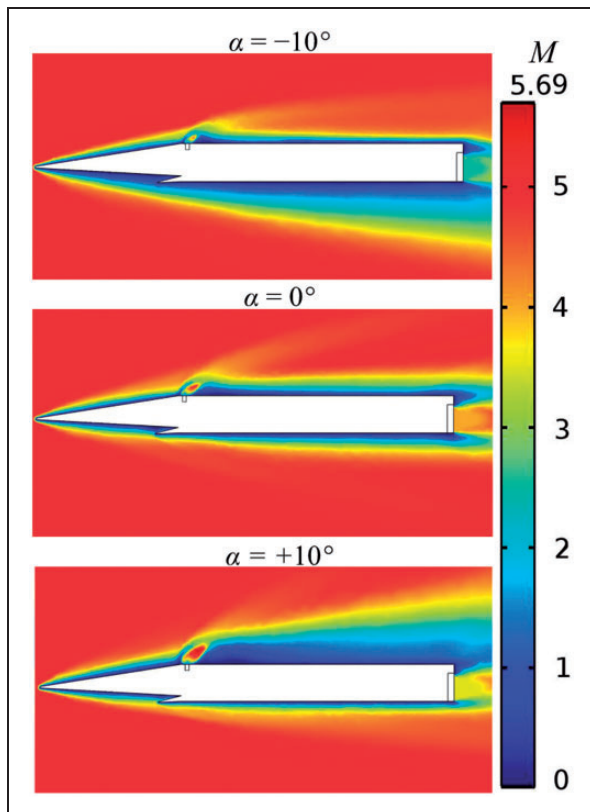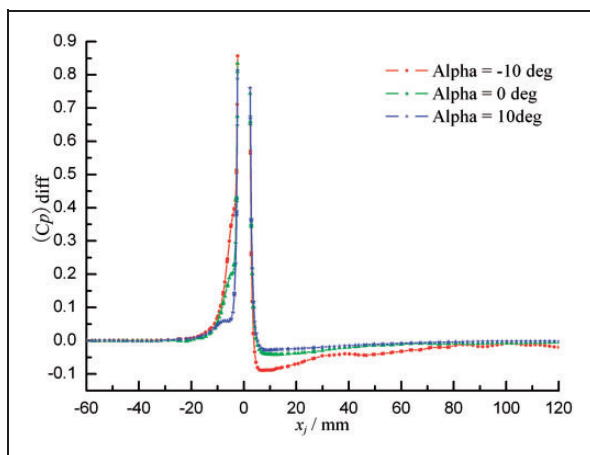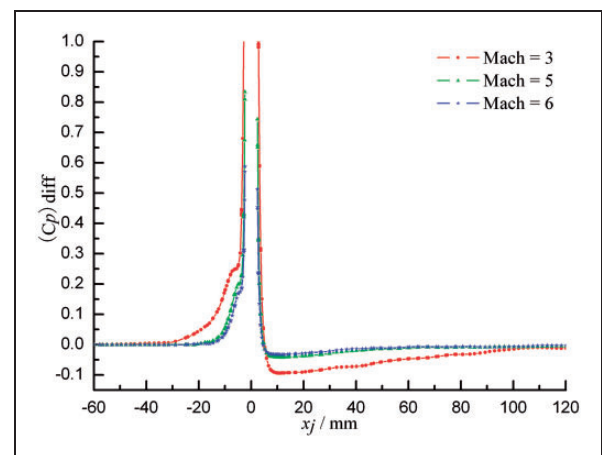
Figure 12. Mach number distribution at different angles of attack.
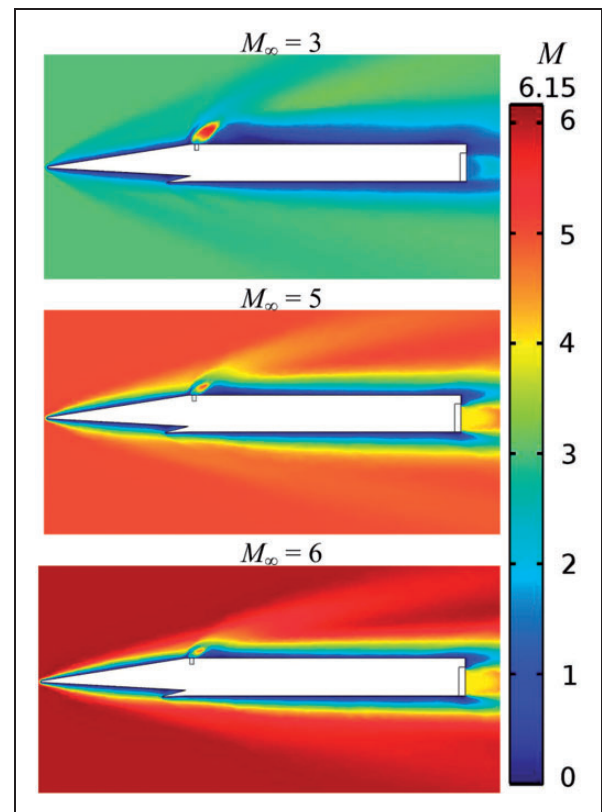
Figure 14. Mach number distribution at different free-stream Mach numbers.

Figure 13. Comparison of pressure distribution at different angles of attack.

Figure 15. Comparison of pressure distribution at different free-stream Mach numbers.

Furthermore, the jet flow expands largely to both sides of the fuselage for GA vehicle, whereas the jet influencing region of QW vehicle concentrates relatively on the upper surface.

The pressure contours near the orifice are shown in Figure 9, and the pressure before the orifice for QW vehicle is higher than that for GA vehicle, due to concentrated jet influencing region of QW vehicle and the diffuse region on each sides of GA vehicle, which has been clarified in the previous section. We can observe it clearly from side-view wall pressure

contours shown in Figure 10, in which the high pressure interference region before the orifice is diffused to the side of GA vehicle. Moreover, the verge of JI region is below the horizontal meridian and gets to the leeward side of the jet, namely, "wrap-around" the vehicle body. This phenomenon results in a weaker effect of the jet. However, the JI region expands barely to the side of QW vehicle. Even though it happens, the pressure on both sides of the vehicle does not lead to a counteraction of the jet force.

In Figure 11, $(C_p)_{\text{diff}}$ along the axial direction at different azimuth angles were drawn. To compare the pressure coefficient difference in front and behind the jet, the jet coordinate system $ox_jy_jz_j$ was established, of which the origin is located on the center of orifice and the direction of every coordinate axis is the same as the primary coordinate system $oxyz$. For the 180° azimuth angle, $(C_p)_{\text{diff}}$ of both vehicles behind the jet are almost identical, whereas the one of QW vehicle before the jet is evidently higher than GA vehicle. $(C_p)_{\text{diff}}$ of QW vehicle is reduced as the azimuth angle decreases. For the azimuth angles of 120° and 90°, the pressure lines are located at the side of QW vehicle, and the $(C_p)_{\text{diff}}$ is close to zero, whereas the one of GA vehicle cannot be neglected. As a consequence, the lateral jet effect of QW vehicle is concentrated on the upper-wall so that it is better than GA vehicle.

Effect of angle of attack

To analysis the lateral jet effect of angle of attack, simulations were implemented in Case 3, and flow Mach number distributions were obtained at three angles −10°, 0°, and 10°. As shown in Figure 12, the jet flow and main stream act on the same side to lead to great interaction with a negative angle of attack. In the case, the separate region before the orifice is reduced to generate stronger bow shock and higher overpressure, whereas behind the orifice it brings more obvious low-pressure region. However, the jet is located in the leeward side with a positive angle of attack, making that main stream has less impact for the jet flow. The barrel shock zone expands, and the bow shock before the orifice gets weak to producing lower overpressure region in this situation.

As shown in Figure 13, with a negative angle of attack, the wall pressure coefficient difference before the jet is increased due to the meridian for $\varphi = 180°$ located in the windward side, while $(C_p)_{\text{diff}}$ behind the jet is decreased. It creates a greater attitude control moment and, therefore, enhances the effect of lateral jet. On the contrary, as the vehicle at a positive angle of attack, the meridian for $\varphi = 180°$ is situated in the leeward side, resulting in a decrease of $(C_p)_{\text{diff}}$ before the jet and an increase behind the jet. Thus, the effect of lateral jet is declining.

Effect of free-stream Mach number

In Cases 2–4, the effects of free-stream Mach number were investigated to get Mach number distributions for three free-stream Mach numbers 3, 5, and 6. From Figure 14, with the increase in the free-stream Mach number, the inflow dynamic pressures increase, and the barrel shock becomes smaller. The jet flow behind the orifice is closer to the vehicle body, which the pressure of low-pressure region increases and the low-pressure point moves forward. Hence,

the effect of lateral jet gets weak. It is also verified by $(C_p)_{\text{diff}}$ along the axial direction in Figure 15. As the free-stream Mach number decreases, there is a larger overpressure region before the orifice with $(C_p)_{\text{diff}}$ increasing and a larger low-pressure region behind the orifice with $(C_p)_{\text{diff}}$ decreasing. As a result, it produces greater attitude control moment and better effect of lateral jet.

Conclusions

Numerical simulations have been conducted to investigate lateral JI effects for the hypersonic QW vehicle. A reasonable jet nozzles layout has been proposed, and comparisons of the JI flow structures have been carried out based on 3D viscous compressible RANS codes. Furthermore, the influences of lateral jet control have been examined for different angles of attack and free-stream Mach numbers. The main contribution of this paper is threefold:

(a) Compared with GA vehicle, the jet influencing region of QW vehicle concentrates relatively on the upper surface and hardly diffuses to the side of body. The "wrap-around" effect, as existing in GA vehicle, is not produced in QW vehicle, resulting in a better effect of lateral jet.

(b) With the increase in angle of attack, the fact is that the barrel shock zone expands, and the bow shock before the orifice gets weakened to induce a decrease of $(C_p)_{\text{diff}}$ and an increase of that behind the orifice. Therefore, the attitude control moment reduces, and the effect of lateral jet lessens.

(c) In the case before the jet, the barrel shock gets smaller as the free-stream Mach number increasing to induce a decrease of $(C_p)_{\text{diff}}$. Furthermore, the pressure of overpressure region reduces, and the overpressure point moves backward. The case behind the jet is just the opposite. Hence, it leads to a lower attitude control moment and a weaker effect of lateral jet.

Conflict of interest

None declared.

References

1. Cassel LA. Applying jet interaction technology. *J Spacecraft Rockets* 2003; 40: 523–537.
2. Dyakonov AA, Glass CE, Desai PN, et al. Analysis of effectiveness of phoenix entry reaction control system. *J Spacecraft Rockets* 2011; 48: 746–755.
3. Alkandry H, Boyd ID, Reed EM, et al. Aerodynamic interactions of reaction-control-system jets for atmospheric entry aeroshells. *AIAA J* 2013; 51: 1105–1118.

4. Aswin G and Chakraborty D. Numerical simulation of transverse side jet interaction with supersonic free stream. *Aero Sci Technol* 2010; 14: 295–301.
5. Zhang J, Cai J and Cui YD. Effect of nozzle shapes on lateral jets in supersonic cross-flows. In: *Proceedings of the 47th aerospace sciences meeting*, AIAA Paper no. 2009-1477, January 2009. doi: 10.2514/6.2009-1477.
6. Lee JW, Min BY, Byun YH, et al. Computational investigation and design optimization of a lateral-jet-controlled missile. *J Aircraft* 2006; 43: 1292–1300.
7. DeSpirito J. Factors affecting reaction jet interaction effects on projectiles. In: *Proceedings of the 29th AIAA applied aerodynamics conference*, AIAA Paper no. 2011-3031, June 2011. doi: 10.2514/6.2011-3031.
8. DeSpirito J. Transient lateral jet interaction effects on a generic fin-stabilized projectile. In: *Proceedings of the 30th AIAA applied aerodynamics conference*, AIAA Paper no. 2012-2907, June 2012. doi: 10.2514/6. 2012-2907.
9. Stahl B, Esch H and Gulhan A. Experimental investigation of side jet interaction with a supersonic cross flow. *Aero Sci Technol* 2008; 12: 269–275.
10. Stahl B, Emunds H and Gulhan A. Experimental investigation of hot and cold side jet interaction with a supersonic cross-flow. *Aero Sci Technol* 2009; 13: 488–496.
11. Cai J, Tsai HM and Liu F. A parallel viscous flow solver on multi-block overset grids. *Comput Fluid* 2006; 35: 1290–1301.
12. Roache PJ. Quantification of uncertainty in computational fluid dynamics. *Annu Rev Fluid Mech* 1997; 29: 123–160.

Nomenclature

Notation

B	breadth of quasi-waverider vehicle fuselage, mm
C_p	pressure coefficient
d	diameter of lateral jet nozzle, mm
D	diameter of cylinder body, mm
M_J	jet exit Mach number
M_∞	free-stream Mach number
P	static pressure, Pa
P_{oj}	jet exit total pressure, Pa
P_∞	free-stream static pressure, Pa
T_t	free-stream total temperature, K
α	angle of attack, (°)
γ	ratio of specific heats
ϕ	azimuth angle (°)

Subscripts

diff	difference between the case with and without jet
with jet	the case with jet
without jet	the case without jet